Chapter 10

Brain Network Analysis from High-Resolution EEG Signals

Fabrizio De Vico Fallani[1,2] and Fabio Babiloni[1,3]

[1]I*RCCS "Fondazione Santa Lucia", Rome, Italy*
[2]*Research Centre for Models and Information Analysis in Biomedical Systems, University "Sapienza", Rome, Italy*
[3]*Department of Human Physiology and Pharmacology, University "Sapienza", Rome, Italy*

Over the last decade, there has been a growing interest in the detection of the functional connectivity in the brain from different neuroelectromagnetic and hemodynamic signals recorded by several neuro-imaging devices such as the functional Magnetic Resonance Imaging (fMRI) scanner, electroencephalography (EEG) and magnetoencephalography (MEG) apparatus. Many methods have been proposed and discussed in the literature with the aim of estimating the functional relationships among different cerebral structures. However, the necessity of an objective comprehension of the network composed by the functional links of different brain regions is assuming an essential role in the Neuroscience. Consequently, there is a wide interest in the development and validation of mathematical tools that are appropriate to spot significant features that could describe concisely the structure of the estimated cerebral networks. The extraction of salient characteristics from brain connectivity patterns is an open challenging topic, since often the estimated cerebral networks have a relative large size and complex structure. Recently, it was realized that the functional connectivity networks estimated from actual brain-imaging technologies (MEG, fMRI and EEG) can be analyzed by means of the graph theory. Since a graph is a mathematical representation of a network, which is essentially reduced to nodes and connections between them, the use of a theoretical graph approach seems relevant and useful as firstly demonstrated on a set of anatomical brain networks. In those studies, the authors have employed two characteristic measures, the *average shortest path L* and the *clustering index C*, to extract respectively the global and local properties of the network structure. They have found that anatomical brain networks exhibit many local connections (i.e. a high *C*) and few random long distance connections (i.e. a low *L*). These values identify a particular model that interpolate between a regular lattice and a random structure. Such a model has been designated as "small-

world" network in analogy with the concept of the small-world phenomenon observed more than 30 years ago in social systems. In a similar way, many types of functional brain networks have been analyzed according to this mathematical approach. In particular, several studies based on different imaging techniques (fMRI, MEG and EEG) have found that the estimated functional networks showed small-world characteristics. In the functional brain connectivity context, these properties have been demonstrated to reflect an optimal architecture for the information processing and propagation among the involved cerebral structures. However, the performance of cognitive and motor tasks as well as the presence of neural diseases has been demonstrated to affect such a small-world topology, as revealed by the significant changes of L and C. Moreover, some functional brain networks have been mostly found to be very unlike the random graphs in their *degree-distribution*, which gives information about the allocation of the functional links within the connectivity pattern. It was demonstrated that the *degree distributions* of these networks follow a power-law trend. For this reason those networks are called "scale-free". They still exhibit the small-world phenomenon but tend to contain few nodes that act as highly connected "hubs". Scale-free networks are known to show resistance to failure, facility of synchronization and fast signal processing. Hence, it would be important to see whether the scaling properties of the functional brain networks are altered under various pathologies or experimental tasks. The present Chapter proposes a theoretical graph approach in order to evaluate the functional connectivity patterns obtained from high-resolution EEG signals. In this way, the "Brain Network Analysis" (in analogy with the Social Network Analysis that has emerged as a key technique in modern sociology) represents an effective methodology improving the comprehension of the complex interactions in the brain.

10.1. Cortical Activity Estimation

High-resolution EEG technology has been developed to enhance the poor spatial information of the EEG activity on the scalp and it gives a measure of the electrical activity on the cortical surface. Principally, this technique involves the use of a larger number of scalp electrodes (64-256). In addition, high-resolution EEG uses realistic MRI-constructed subject head models and spatial de-convolution estimations which are commonly computed by solving a linear inverse problem based on boundary-element mathematics. In the present study, the cortical activity was estimated from EEG recordings by using a realistic head model, whose cortical surface consisted of about 5000 triangles disposed uniformly.

Each triangle represents the electrical dipole of a particular neuronal population and the estimation of its current density was computed by solving the linear inverse problem according to techniques described in previous works. In

this way, the electrical activity in different Regions Of Interest (ROIs) can be obtained by averaging the current density of the various dipoles within the considered cortical area.

10.1.1. *Head models and regions of interest*

In order to estimate cortical activity from conventional EEG scalp recordings, realistic head models reconstructed from T1-weighted MRIs are employed. Scalp, skull and dura mater compartments are segmented from MRIs and tessellated with about 5000 triangles. Then, the cortical regions of interest (ROIs) are drawn by a neuroradiologist on the computer-based cortical reconstruction of the individual head model by following a Brodmann's mapping criterion.

10.1.2. *Estimation of cortical source current density*

The solution of the following linear system:

$$Ax = b + n \tag{10.1}$$

provides an estimation of the dipole source configuration x which generates the measured EEG potential distribution b. The system includes also the measurement noise n, assumed to be normally distributed. A is the lead field matrix, where each *j-th* column describes the potential distribution generated on the scalp electrodes by the *j-th* unitary dipole. The current density solution vector ξ of Eq. (10.1) was obtained as:

$$\xi = \arg\min_{x} \left(\| \mathbf{A}x - b \|_{\mathbf{M}}^2 + \lambda^2 \| x \|_{\mathbf{N}}^2 \right) \tag{10.2}$$

where M, N are matrices associated to the metrics of data and source space, respectively; λ is a regularization parameter; $\| \ldots \|_{\mathrm{M}}$ represent the M-norm of the data space b and $\| \ldots \|_{\mathrm{N}}$ the N-norm of the solutions space x. The formula (10.2) represents a minimization problem also known as *linear inverse* problem.

As a metric of the data space the identity matrix is generally employed. However, the metric in the source space can be opportunely modified when hemodynamic information is available from recorded fMRI data. This aspect can notably improve the localization of the source activity. An estimate of the signed magnitude of the dipolar moment for each one of the 5000 cortical dipoles was then obtained for each time point. The instantaneous average of all the dipoles' magnitude within a particular ROI was used to estimate the average cortical activity in that ROI during the whole time interval of the experimental task.

Figure 10.1 illustrates the effect of the linear inverse problem's solution. From a scalp potential distribution one can estimate accurately the original cortical potential.

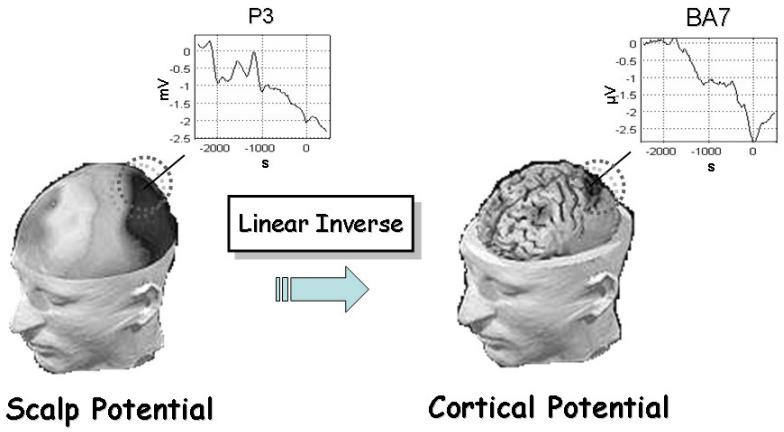

Fig. 10.1. Electrical activity estimation in the Brodmann area 7 from the scalp measurement in the parietal sensor P3.

10.2. Functional Connectivity Estimation

Among the linear and nonlinear methods used to estimate functional brain connectivity, frequency-based methods are particularly attractive for the analysis of EEG or MEG data, since the activity of neural populations is often best expressed in this domain. Many EEG and/or MEG frequency-based methods that have been proposed in recent years for assessment of the directional influence of one signal on another are based mainly on the Granger theory of causality. Granger theory mathematically defines what a "causal" relation between two signals is. According to this theory, an observed time series x(n) is said to cause another series y(n) if the knowledge of x(n)'s past significantly improves prediction of y(n); this relation between time series is not necessarily reciprocal, i.e., x(n) may cause y(n) without y(n) causing x(n). This lack of reciprocity allows the evaluation of the direction of information flow between structures. Kaminski and Blinowska proposed a multivariate spectral measure, called the Directed Transfer Function (DTF), which can be used to determine the directional influences between any given pair of channels in a multivariate dataset. DTF is an estimator that simultaneously characterizes the direction and spectral properties of the interaction between brain signals and requires only one multivariate autoregressive (MVAR) model to be estimated simultaneously from

all the time series. The advantages of MVAR modeling of multichannel EEG signals in order to compute efficient connectivity estimates have recently been stressed. Kus *et al.* demonstrated the superiority of MVAR multichannel modeling with respect to the pair-wise autoregressive approach. Another popular estimator, the Partial Directed Coherence (PDC), based on MVAR coefficients transformed into the frequency domain was recently proposed, as a factorization of the Partial Coherence. The PDC is of particular interest because of its ability to distinguish direct and indirect causality flows in the estimated connectivity pattern. If another "true" flow exists from region *x2* to region *x3*, the PDC estimator does not add an "erroneous" causality flow between the signal recorded from region *x1* to region *x3*. This property is particularly interesting in its application to brain signals, where the interpretation of a direct connection between two cortical regions is straightforward.

10.2.1. *MultiVariate AutoRegressive models*

The approach based on multivariate autoregressive models (MVAR) can simultaneously model a whole set of signals. Let X be a set of estimated cortical time series:

$$X = [x_1(t), x_2(t), ..., x_N(t)] \tag{10.3}$$

where t refers to time and N is the number of cortical areas considered. Given an MVAR process which is an adequate description of the data set X:

$$\sum_{k=0}^{p} \Lambda(k) X(t-k) = E(t) \tag{10.4}$$

where $X(t)$ is the data vector in time; $E(t) = [e_1(t), \ldots, e_N]$ is a vector of multivariate zero-mean uncorrelated white noise processes; $\Lambda(1)$, $\Lambda(2), \ldots, \Lambda(p)$ are the $N \times N$ matrices of model coefficients ($\Lambda(0) = I$); and p is the model order. The p order is chosen by means of the Akaike Information Criteria (AIC) for MVAR processes. In order to investigate the spectral properties of the examined process, the Eq. (10.4) is transformed into the frequency domain:

$$\Lambda(f) X(f) = E(f) \tag{10.5}$$

where:

$$\Lambda(f) = \sum_{k=0}^{p} \Lambda(k) e^{-j2\pi f \Delta t k} \tag{10.6}$$

and Δt is the temporal interval between two samples. Eq. (10.5) can then be rewritten as:

$$X(f) = \Lambda^{-1}(f)E(f) = H(f)E(f) \tag{10.7}$$

$H(f)$ is the transfer matrix of the system, whose element H_{ij} represents the connection between the *j-th* input and the *i-th* output of the system.

10.2.1.1. *Directed transfer function*

The Directed Transfer Function, representing the causal influence of the cortical waveform estimated in the *j-th* ROI on that estimated in the *i-th* ROI is defined in terms of elements of the transfer matrix *H*, is:

$$\theta_{ij}^2(f) = \left|H_{ij}(f)\right|^2 \tag{10.8}$$

In order to compare the results obtained for cortical waveforms with different power spectra, normalization can be performed by dividing each estimated DTF by the squared sums of all elements of the relevant row, thus obtaining the so-called normalized DTF:

$$\gamma_{ij}^2(f) = \frac{\left|H_{ij}(f)\right|^2}{\sum_{m=1}^{N}\left|H_{im}(f)\right|^2} \tag{10.9}$$

$\gamma^2_{ij}(f)$ expresses the ratio of influence of the cortical waveform estimated in the *j-th* ROI on the cortical waveform estimated in the *i-th* ROI, with respect to the influence of all the estimated cortical waveforms. Normalized DTF values are in the interval [0 1], and the normalization condition:

$$\sum_{n=1}^{N}\gamma_{in}^2(f) = 1 \tag{10.10}$$

is applied.

10.2.1.2. *Partial directed coherence*

In order to distinguish between direct and cascade flows, another estimator describing the direct causal relations between signals, the Partial Directed Coherence (PDC), was proposed in 2001. Like DTF, it is defined in terms of MVAR coefficients transformed to the frequency domain. The definition of Partial Directed Coherence (PDC) is:

$$\pi_{ij}(f) = \frac{\Lambda_{ij}(f)}{\sqrt{\sum_{k=1}^{N} \Lambda_{ki}(f)\Lambda_{kj}^{*}(f)}} \tag{10.11}$$

The PDC from j to i, $\pi_{ij}(f)$, describes the directional flow of information from the activity in the ROI $x_j(t)$ to the activity in $x_i(t)$, whereupon common effects produced by other ROIs $x_k(t)$ on the latter are subtracted leaving only a description that is exclusive from $x_j(t)$ to $x_i(t)$. PDC values are in the interval [0 1] and the normalization condition:

$$\sum_{n=1}^{N} \left|\pi_{ni}(f)\right|^2 = 1 \tag{10.12}$$

is verified. According to this condition, $\pi_{ij}(f)$ represents the fraction of the time evolution of ROI j directed to ROI i, as compared to all of j's interactions with other ROIs. Figure 10.2 shows a schematic representation of the functional connectivity estimation from a set of high-resolution EEG signals to the cortical network.

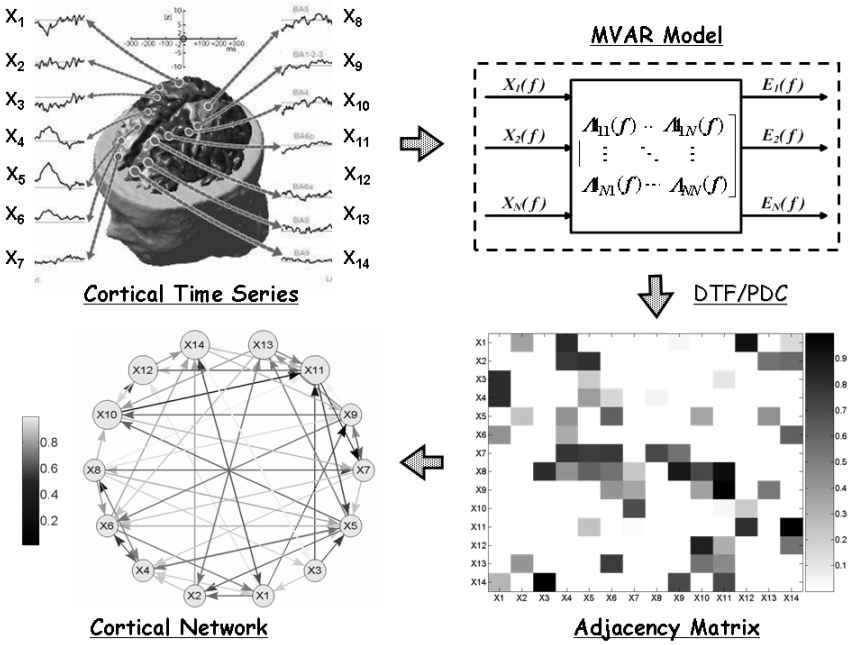

Fig. 10.2. From a set of cortical time series the MVAR method estimates in the frequency domain a functional connectivity pattern that can be modeled by means of a graph.

10.2.2. *Adaptive MVAR models*

Among the multivariate methods, the Directed Transfer Function (DTF) and the Partial Directed Coherence are estimators characterizing, at the same time, direction and spectral properties of the interaction between brain signals, and require only one MVAR model to be estimated from all the time series. However, the classical estimation of these methods requires the stationarity of the signals; moreover, with the estimation of a unique MVAR model on an entire time interval, transient pathways of information transfer remains hidden. This limitation could bias the physiologic interpretation of the results obtained with the connectivity technique employed. To overcome this limitation, different algorithms for the estimation of MVAR with time dependent coefficients were recently developed. Ding *et al*., used a short-time windows technique, which requires the stationarity of the signal within short-time windows.

Hesse *et al*., proposed an application to MVAR estimation of the extension of the recursive least squares (RLS) algorithm with a forgetting factor. This estimation procedure allows for the simultaneous fit of one mean MVAR model to a set of single trials, each one representing a measurement of the same task. In contrast to short-window techniques, the multi-trial RLS algorithm does not require the stationarity of the signals, and involves the information of the actual past of the signal, whose influence decreases exponentially with the time distance to the actual samples. The advantages of this estimation technique are an effective computation algorithm and a high adaptation capability. It was demonstrated in that the adaptation capability of the estimation (measured by its adaptation speed and variance) does not depend on the model dimension.

10.3. Graph Theory

A graph is an abstract representation of a network. It consists of a set of vertices (or nodes) and a set of edges (or connections) indicating the presence of some of interaction between the vertices. The adjacency matrix A contains the information about the connectivity structure of the graph. When a weighted and directed edge exists from the node i to j, the corresponding entry of the adjacency matrix is $A_{ij} \neq 0$; otherwise $A_{ij} = 0$.

10.3.1. *Network density*

The simplest attribute for a graph is its density k, defined as the actual number of connections within the model divided by its maximal capacity; density ranges

from 0 to 1, the sparser is a graph, the lower is its value. When dealing with weighted networks, a useful generalization of this quantity is represented by the weighted-density k_w, which evaluates the intensities of the links composing the network. The mathematical formulation of the network density is given by the following:

$$k_w(A) = \sum_{i \neq j \in V} w_{ij} \tag{10.13}$$

Where A is the adjacency matrix and w_{ij} is the weight of the respective arc from the point j to the point i. $V=1…N$ is the set of nodes within the graph.

10.3.2. *Node strength*

In the same way, the simplest attribute of a node is its connectivity degree, which is the total number of connections with other vertices. In a weighted graph, the natural generalization of the degree of a node i is the node strength or node weight or weighted-degree. This quantity has to be split into in-strength s_{in} and out-strength s_{out}, when directed relationships are being considered. The strength index integrates the information of the links' number (degrees) with the connections' weight, thus representing the total amount of outgoing intensity from a node or incident intensity into it. The formulation of the in-strength index s_{in} can be introduced as follows:

$$s_{in}(i) = \sum_{j \in V} w_{ij} \tag{10.14}$$

It represents the whole functional flow incoming to the vertex i. V is the set of the available nodes and w_{ij} is the weight of the particular arc from the point j to the point i. In a similar way, for the out-strength:

$$s_{out}(i) = \sum_{j \in V} w_{ji} \tag{10.15}$$

It represents the whole functional flow outgoing from the vertex i.

10.3.3. *Strength distributions*

For a weighted graph, the arithmetical average of all the nodes' strengths $<s>$ only gives little information about the distributions of the links intensity within the system. Hence, it is useful to introduce $R(s)$ as the fraction of vertices in the graph that have strength equal to s. In the same way, $R(s)$ is the probability that a

vertex chosen uniformly at random has weight = s. A plot of $R(s)$ for any network can be constructed by making a histogram of the vertices' strength. This histogram represents the strength distribution of the graph and allows a better understanding of the strength allocation in the system. In particular, when dealing with directed graphs, the strength distribution has to be split in order to consider in a separated way the contribution of the incoming and outgoing flows.

10.3.4. *Link Reciprocity*

In a directed network, the analysis of *link reciprocity* reflects the tendency of vertex pairs to form mutual connections between each other [44]. Here we computed the correlation coefficient index ρ proposed by Garlaschelli and Loffredo, which measures whether double links (with opposite directions) occur between vertex pairs more or less often than expected by chance. The correlation coefficient can be written as follows:

$$\rho(A) = \frac{r(A) - k_w(A)}{1 - k_w(A)} \tag{10.16}$$

In this formula, r is the ratio between the number of links pointing in both directions and the total number of links, while k_w is the connection density that equals the average probability of finding a reciprocal link between two connected vertices in a random network. As a measure of reciprocity, ρ is an absolute quantity that directly allows one to distinguish between reciprocal ($\rho > 0$) and anti-reciprocal ($\rho < 0$) networks, with mutual links occurring more and less often than random, respectively. The neutral or areciprocal case corresponds to $\rho = 0$. Note that if all links occur in reciprocal pairs one has $\rho = 1$, as expected.

10.3.5. *Motifs*

By motif it is usually meant a small connected graph of M vertices and a set of edges forming a subgraph of a larger network with N > M nodes. For each N, there are a limited number of distinct motifs. For N = 3, 4, and 5, the corresponding numbers of directed motifs is 13, 199, and 9364. In this work, we focus on directed motifs with N = 3. The 13 different 3-node directed motifs are shown in Fig. 10.3. Counting how many times a motif appears in a given network yields a frequency spectrum that contains important information on the network basic building blocks. Eventually, one can looks at those motifs within the considered network that occur at a frequency significantly higher than in random graphs.

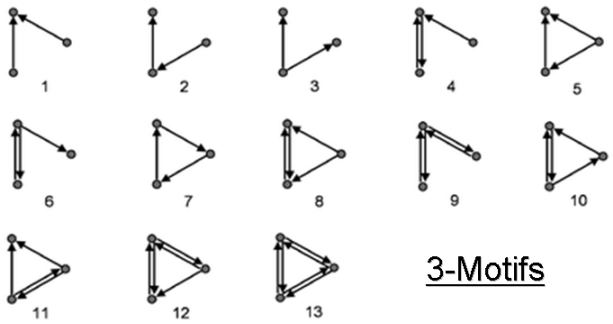

Fig. 10.3. The 13 possible schemes of connectivity that can be achieved in a graph of 3 nodes.

10.3.6. *Network structure*

Two measures are frequently used to characterize the local and global structure of unweighted graphs: the average shortest path L and the clustering index C. The former measures the efficiency of the passage of information among the nodes, the latter indicates the tendency of the network to form highly connected clusters of vertices. Recently, a more general setup has been examined in order to investigate weighted networks. In particular, Latora and Marchiori considered weighted networks and defined the efficiency coefficient e of the path between two vertices as the inverse of the shortest distance between the vertices (note that in weighted graphs the shortest path is not necessarily the path with the smallest number of edges). In the case where a path does not exist, the distance is infinite and $e = 0$. The average of all the pair-wise efficiencies e_{ij} is the global-efficiency E_g of the graph. Thus, global-efficiency can be defined as:

$$E_g(A) = \frac{1}{N(N-1)} \sum_{i \neq j \in V} \frac{1}{d_{i,j}} \tag{10.17}$$

where N is the number of vertices composing the graph. Since the efficiency e also applies to disconnected graphs, the local properties of the graph can be characterized by evaluating for every vertex i the efficiency coefficients of $\boldsymbol{A}i$, which is the sub-graph composed by the neighbors of the node i. The local-efficiency E_l is the average of all the sub-graphs global-efficiencies:

$$E_l(A) = \frac{1}{N} \sum_{i \in V} E_{glob}(A_i) \tag{10.18}$$

Since the node i does not belong to the sub-graph $\boldsymbol{A}i$, this measure reveals the level of fault-tolerance of the system, showing how the communication is efficient between the first neighbors of i when i is removed. Global- (E_g) and local-efficiency (E_l) were demonstrated to reflect the same properties of the inverse of the average shortest path $1/L$ and the clustering index C. In addition, this new definition is attractive since it takes into account the full information contained in the weighted links of the graph and provides an elegant solution to handle disconnected vertices.

10.4. Application to Real Data

In the following, two applications are presented in order to study the significant features of the functional connectivity networks estimated with the use of advanced high-resolution EEG methodologies.

10.4.1. *Cortical network structure in tetraplegics*

The first study aims at analyzing the structure of cortical connectivity during the attempt to move a paralyzed limb by a group of spinal cord injured patients. Five healthy (CTRL) subjects and five spinal cord injured (SCI) patients participated to the present study. In particular, spinal cord injuries were of traumatic etiology and located at the cervical level (C6 in three cases, C5 and C7 in two cases, respectively); patients had not suffered for a head or brain lesion associated with the trauma leading to the injury. The informed consent statement was signed by each patient after the explanation of the study, which was approved by the local institutional ethics committee. For the EEG data acquisition, subjects were comfortably seated on a reclining chair, in an electrically shielded and dimly lit room. They were asked to perform a brisk protrusion of their lips while they were performing (healthy subjects) or attempting (SCI patients) a right foot movement. By means of the lips protrusion, the SCI patients provided an evident trigger in correspondence of their attempt to move. For each subject, the cortical activity was estimated according to the high-resolution EEG technique (see paragraph X.1). By using the passage through the Tailairach coordinates system, twelve Regions Of Interest (ROIs) were then obtained by segmentation of the Brodmann areas (B.A.) on the accurate cortical model utilized for each subject. Bilateral ROIs considered in this analysis are the primary motor areas for foot (MIF) and lip movement (MIL), the proper supplementary motor area (SMAp), the standard pre-motor area (BA6), the cingulated motor area (CMA) and the associative area (BA7).

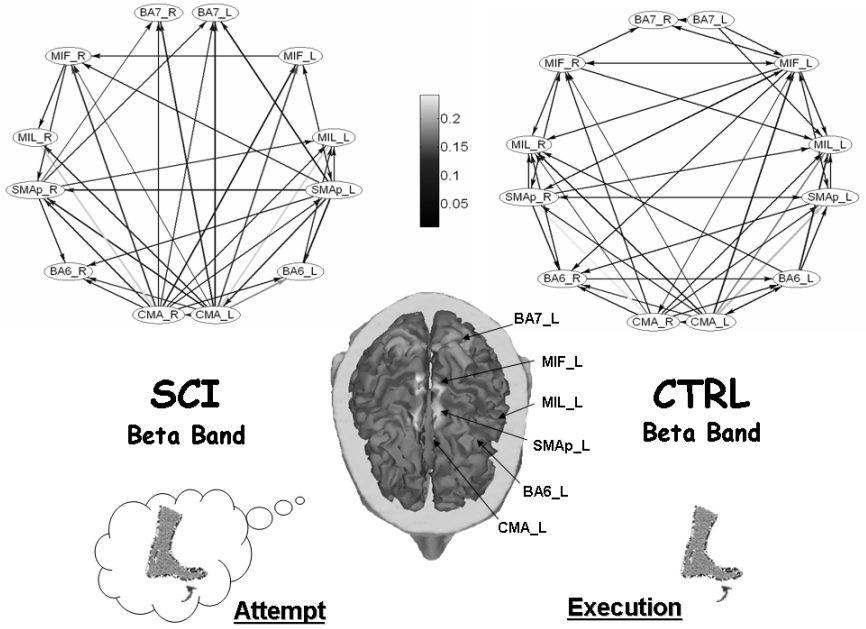

Fig. 10.4. (Up) Average cortical networks in the Beta band for the SCI group and CTRL group. (Centre*)* Location of the ROIs on the realistic cortex model of a representative subject. (Bottom) The SCI group attempted the foot movement, while the CTRL group executed it.

In order to study the preparation to an intended foot movement, a time segment of 1.5 seconds before the lips pursing was analyzed. The lips movement was detected by means of an EMG. The task was repeated every 6-7 seconds, in a self-paced manner, and the 100 single trials recorded will be used for the estimate of functional connectivity by means of the Directed Transfer Function (DTF, see paragraph X.2) in four frequency bands (Theta 4-7 Hz, Alpha 8-12 Hz, Beta 13-29 Hz, 30-40 Hz). Only the connections that were statistically significant (at $p < 0.001$) after a contrast with a surrogate distribution of one thousand DTF values among the same ROIs were considered for the network to be analyzed with graph theory's tools. Figure 10.4 shows the average cortical network estimated in the Beta frequency band for the SCI group and for the CTRL group, during the motor attempt/execution of the task. The twelve ROIs (the nodes of the cortical network) are indicated on the cortex of one representative subject.

The upper panels of Fig. 10.5 show the average in- and out-degree in the SCI population a) and in the CTRL group b) for the significant Beta band. Direct comparisons of the data show that in the SCI patients the number of links

outgoing from both the SMAp areas Left and Right is largely higher than the CTRL subjects. This result puts in evidence the important role of the supplementary motor areas (SMAp Left and Right) that increase their outgoing functional flows to support the diminished activity of their primary motor areas (MIF Left and Right) during the preparation of this motor act.

The panels at the bottom of Fig. 10.5 show the average profiles of the degree distributions for SCI and CTRL group, in the Beta frequency band. An interesting result is that in-degree and out-degree distributions show different trends within each group.

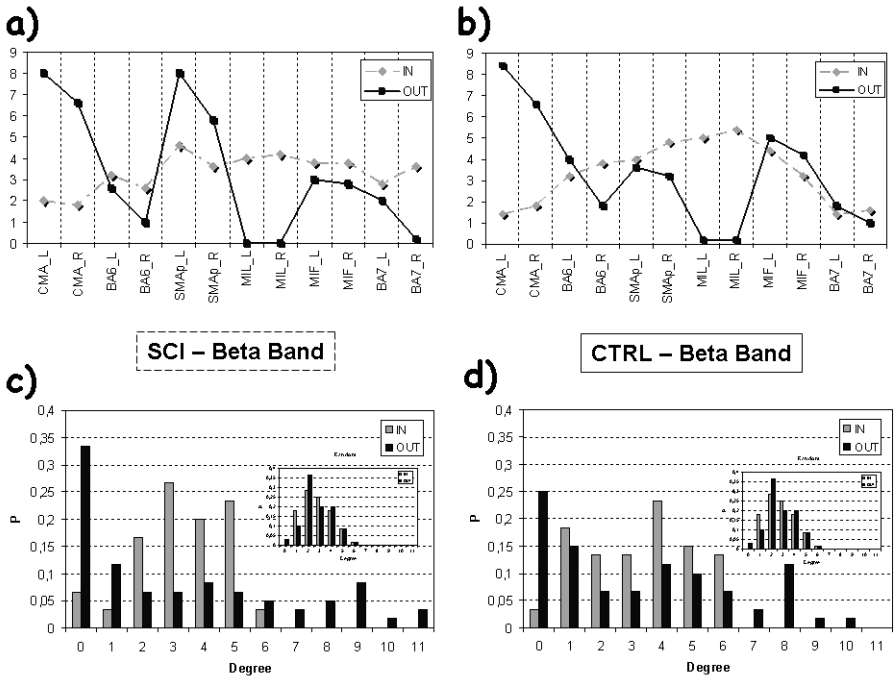

Fig. 10.5. (a) Average in- and out-degrees for the SCI group in the Beta frequency band. (b) Average in- and out-degrees for the CTRL group in the Beta frequency band. (c) Average in- and out-degree distributions for the SCI group in the Beta frequency band. *(*d) Average in- and out-degrees distributions for the CTRL group in the Beta frequency band.

Right-skew tails of out-degree distributions indicates the presence of few nodes with a very high level of outgoing connections, while for the in-degree distributions there are no ROIs in the network with more than six incoming connections. The inset in each figure illustrates the typical Gaussian profile of the degree-distributions in random graphs, which appears to be different from

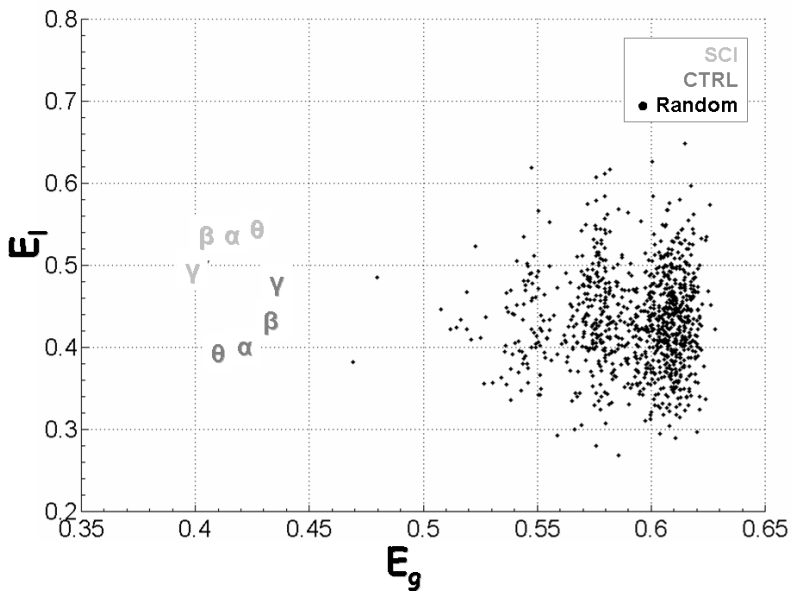

Fig. 10.6. Scatter plot of global- and local-efficiency for SCI networks, CTRL networks and random networks. The Greek symbol codes the average value in a particular frequency band. Black dots identify the values from a distribution of 1000 random graphs.

the estimated cortical networks. Figure 10.6 shows the contrast between the values of global and local efficiency obtained in the two studied populations with those obtained in a set of one thousand random graphs, having the same number of nodes and arcs.

Analysis of variance (ANOVA $p = 0.05$) was used in order to find significant differences between the indices of efficiency indexes computed in the two groups (SCI, CTRL) for all the frequency bands (Theta, Alpha, Beta and Gamma). ANOVA performed on the global-efficiency E_g variable showed no significant differences for the main factors GROUP and BAND. Instead, the ANOVA performed on the E_l variable revealed a strong influence of the between factor GROUP ($F = 32.67$, $p = 0.00045$); while the BAND factor and the interaction between GROUP X BAND were found not significant ($F = 0.21$ and $F = 0.91$ respectively, p values equal to 0.891 and 0.457). Post-hoc tests revealed a significant difference between the two examined experimental groups (SCI, CTRL) in Theta, Alpha and Beta band ($p = 0.006$, 0.01, 0.03 respectively). It can be observed (Fig. 10.6) that the average values of the local efficiency in the SCI subjects are significantly higher than those obtained in the CTRL group, for these three frequency bands. The higher value of local efficiency E_l implies that the network tends to form clusters of ROIs which hold an efficient communication.

These efficient clusters, noticed in the SCI group, could represent a compensative mechanism as a consequence of the partial alteration in the primary motor areas (MIF) due to the effects of the spinal cord injury. Moreover, the estimated cortical networks are not structured like random networks. The statistical contrasts performed by separate Z-tests (Bonferroni corrected for multiple comparisons, $p = 0.05$) were summarized in the Table 10.1.

By inspecting the data presented in both Table 10.1 and Fig. 10.6, it is clear that in general the cortical networks exhibited ordered and regular properties. In particular, the global efficiency is significantly lower than the random mean value, while the local efficiency of the SCI group is significantly higher than random graphs in each band, meaning fault tolerance is privileged with respect to global communication.

Table 10.1. Z-scores of E_g and E_l from the contrasts with 1000 random graphs.

Z Values	SCI-Theta	SCI-Alpha	SCI-Beta	SCI-Gamma	Healthy-Theta	Healthy-Alpha	Healthy-Beta	Healthy-Gamma
E_g	–237.45	–250.13	–262.88	–267.07	–249.81	–238.21	–225.95	–223.4
E_l	57.714	53.314	57.025	38.936	–15.99	–11.051	7.163	21.674

10.4.2. *Time-varying cortical network during foot movement*

The second study intends to evaluate the dynamics of the cerebral networks during the preparation and the execution of the foot movement in healthy subjects. Five voluntary subjects participated to the study (age, 26-32 years; five males). For the EEG data acquisitions, the participants were comfortably seated on a reclining chair in an electrically shielded and dimly lit room. They were asked to perform a dorsal flexion of their right foot, whose preference was previously attested by simple questionnaires (Chapman 1987). The movement task was repeated every 8 seconds, in a self-paced manner and 200 single trials were recorded by using 200 Hz of sampling frequency. Cortical activity was estimated through high-resolution EEG techniques (see paragraph X.1). The ROIs considered for the left (_L) and right (_R) hemisphere are the primary motor areas of the foot (MF_L and MF_R), the proper supplementary motor areas (SM_L and SM_R) and the cingulate motor areas (CM_L and CM_R). The bilateral Brodmann areas 6 (6_L and 6_R), 7 (7_L and 7_R), 8 (8_L and 8_R), 9 (9_L and 9_R) and 40 (40_L and 40_R) were also considered. In order to inspect the brain dynamics during the preparation and the execution of the studied movement, a time segment of 2 seconds was analyzed, after having

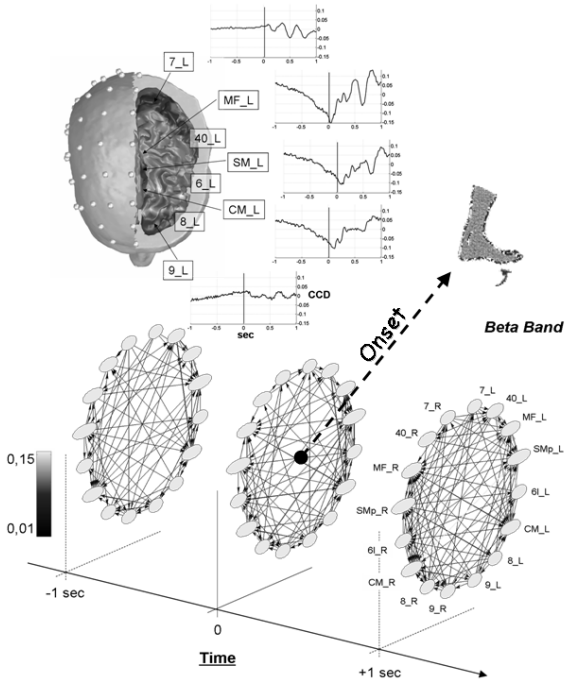

Fig. 10.7. (Up) Realistic head model for a representative subject and cortical activity for the ROIs in the left hemisphere. (Bottom) Three-dimensional representation of the estimated time-varying network in the Beta band for the same subject.

centered it on the onset detected by a tibial EMG. The use of the time-varying Partial Directed Coherence (PDC, see paragraph X.2) to the cortical waveforms obtained from EEG signals returned a cortical network for each selected time sample and frequency band. In order to consider only those task-related connections, a filtering procedure based on statistical validation was adopted. In each trial, a rest period of 2 seconds preceding the movement was selected as an element of contrast (from -4 to -2 s before the onset, i.e. the moment in which the movement occurs). Figure 10.7 illustrates the locations of the regions of interest (ROIs) on the left hemisphere of the cortex model together with their estimated temporal activity. At the bottom, the time-varying cortical network in the Beta frequency band is shown for a representative subject. In particular, three instants are highlighted; one second before the onset, the onset itself and one second after the onset.

Figure 10.8a) shows the in-strength values for the average network during three moments of interest that presented significant differences from random networks. Among all the cortical regions, the supplementary motor areas of both

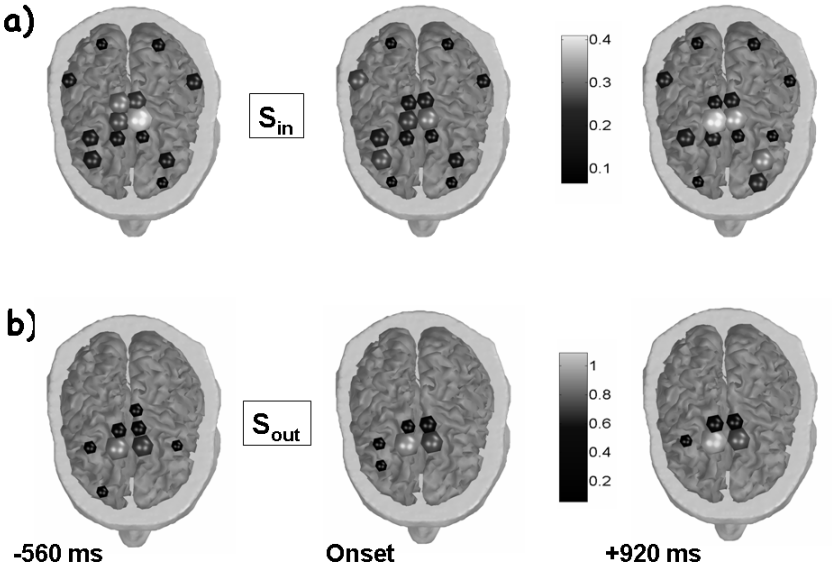

Fig. 10.8. Average in- and out-strength in the Beta band during three significant moments. The little spheres are located in correspondence of each ROI. The size and color of each sphere encodes the degree value.

hemispheres (SM_L and SM_R) show the highest values of in-strength index. In the time points that precedes the onset movement (-560 ms) also the right and left primary motor areas of the foot (MF_L and MF_R) present a considerable number of incoming functional links. Figure 10.8b) shows the average values of out-strength obtained during the three time points of interest. In this particular case, it is evident that the large part of the cortical areas does not produce outgoing edges, while the bilateral cingulate motor region (CM_L and CM_R) presents very high out-strength values. All the indexes calculated on the cortical networks were standardized by considering their Z-score with respect to the distribution obtained from 50 random graphs.

Figure 10.9 shows the average Z values in the analyzed population for the time-varying in- strength R_{in} and out-strength R_{out} distributions in the representative Beta frequency band. An interesting result is that in-strength (R_{in}) and out-strength (R_{out}) distributions show different characteristics. The high Z-scores in correspondence with the high values of S_{out} (i.e. the "right tail" of the distribution) suggest the presence of few ROIs with a very high level of outgoing flows, which makes them act as cortical "hubs". In particular, the intensity of their outgoing links seems to increase as time elapses from the movement

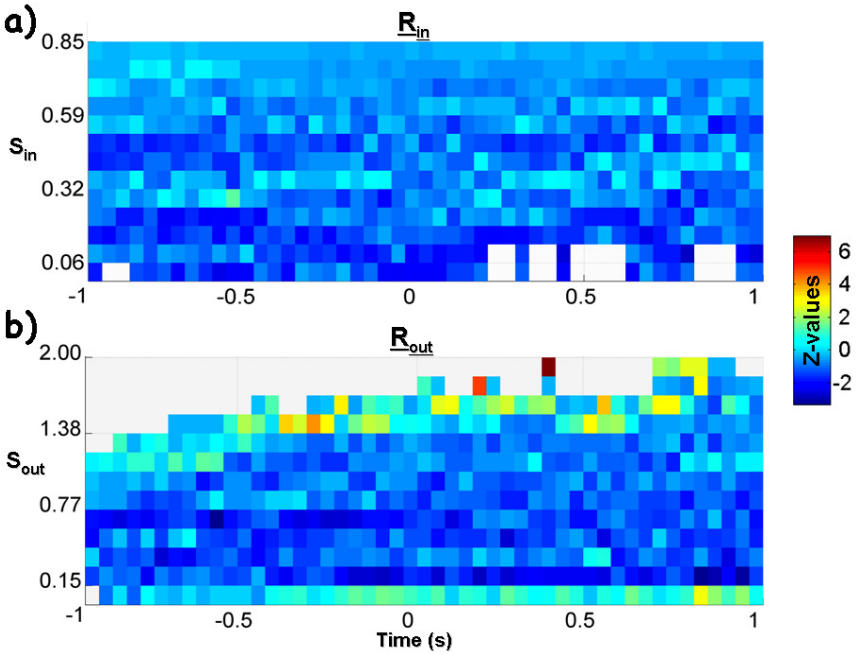

Fig. 10.9. (a) Average time-varying in-strength distributions fro the Beta band. The latency from the movement onset is shown on the x-axes; the in-strength (S_{in}) values on the y-axes. The colour encodes the group-averaged intensity of the R_{in} Z-score. (b) Average time-varying out-strength distributions fro the Beta band. Same conventions as above.

preparation to the movement execution, as revealed by the respective shift of the significant Z values towards high levels of out-strength.

The level of organization in the time-varying cortical networks during the foot movement was analyzed by computing the efficiency indexes E_g and E_l. The E_g and E_l indexes estimated in every subject from the respective cortical networks were contrasted with the ones obtained from the respective random structures. Figure 10.10 shows the average Z-scores of the time-varying E_g (solid line) and E_l - (dotted line) of the connectivity patterns in the Beta frequency band. In particular, one second before the onset (from about -1 to -0.5 *s*), the cortical networks mostly show low values of E_g and E_l, reflecting a weak pattern of communication characterized by long average distances and few clustering connections between the ROIs. Throughout the period closer to the execution of the movement (from about -0.5 *s* to the onset), both the global and local properties increase and in correspondence with it, we observe high values of E_g and E_l.

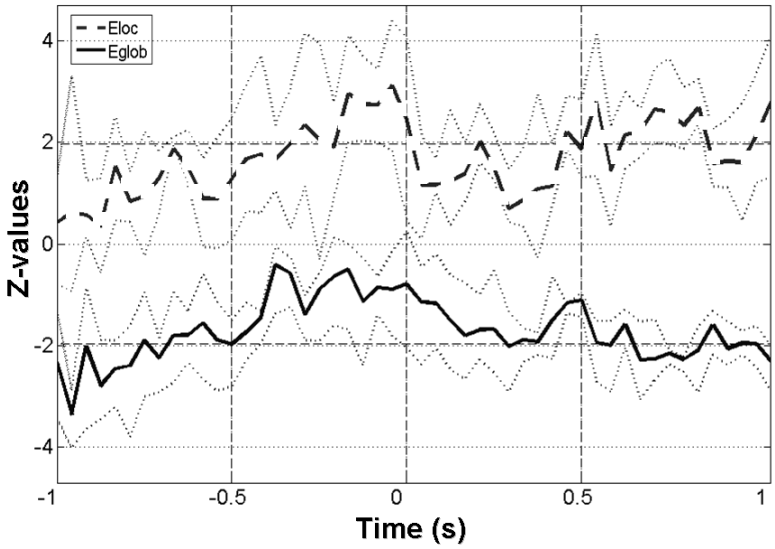

Fig. 10.10. Average time-varying efficiency indexes. The lighter lines around the mean value indicate the time courses of the 25th and 75th percentile. The latency from the movement onset is shown on the x-axes.

Consequently the structure of the cortical networks tends to maximize the interplay between the global integration and its local interactions. This particular structure represents one of the best way in which the cortical areas communicate, since the relevant network presents simultaneously short links between each pair of ROIs and highly connected clusters (i.e. small-world architecture). After the onset (from the onset to +0.5 *s*), the estimated cortical networks show a typical random organization of the functional links, with a high E_g and a low E_l, reflecting the dense presence of wide-scope interactions among the ROIs, but a low tendency of the same cortical regions to form functional clusters. In the last period of the movement execution (from about +0.5 to +1 *s*) the estimated cortical networks mainly show high E_l values and low E_g values. The resulting structure is known to reflect the properties of regular and ordered graphs in which the local property of clustering is privileged with respect to the overall communication. Figure 10.11(a) shows the average time-varying course of the weighted-density k_w in the Beta band during the analyzed period of interest.

In particular, the average intensity of the network links during the preparation (from -0.5 *s* to the onset) is relatively low if compared with its maximum value reached in the following movement execution. In correspondence with this period the network structure presents the most efficient pattern of communication, as revealed by the estimated small-world characteristic.

Therefore, it is interesting to note that the optimal organization of the functional links among the cortical areas during the preparation of the foot movement is not correlated to the need of a high level of overall connectivity.

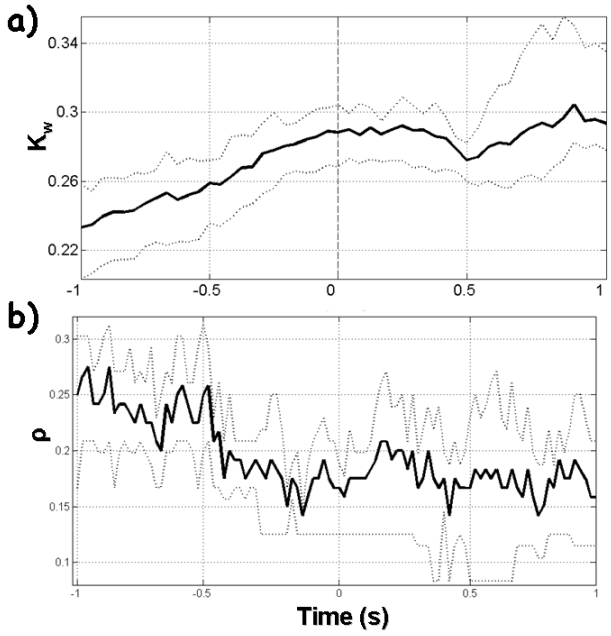

Fig. 10.11. (a) Average time-varying "weighted-density" in the Beta band. (b) Average time-varying "reciprocity" during the period of interest in the Beta band. On y-axes the correlation coefficient ρ while time in seconds on x-axes.

The analysis of the average time-varying reciprocity index revealed an interesting behavior during the preparation (from about -1 to 0 *s*) of the movement in the Beta frequency band. In such a period, the functional network moved from a reciprocal (r = 0.1) to an anti-reciprocal (r = -0.1) state. This aspect emphasizes the role of the early preparation in which a high level of mutual exchange of information is required to speed up the cortical process in expectation of the execution. Moreover, by tracking the evolving involvement of each single reciprocal connection (see Fig. 10.12(a)) it is possible to observe their "persistence" during the entire period of interest. In particular, the persistent bilateral links between the cingulate motor areas and the supplementary motor areas (they correspond to the rows 58 and 69) in the Beta band reveals a novel aspect of such a connection that anyway was expected in a self-paced modality of movement generation, as in our experimental condition.

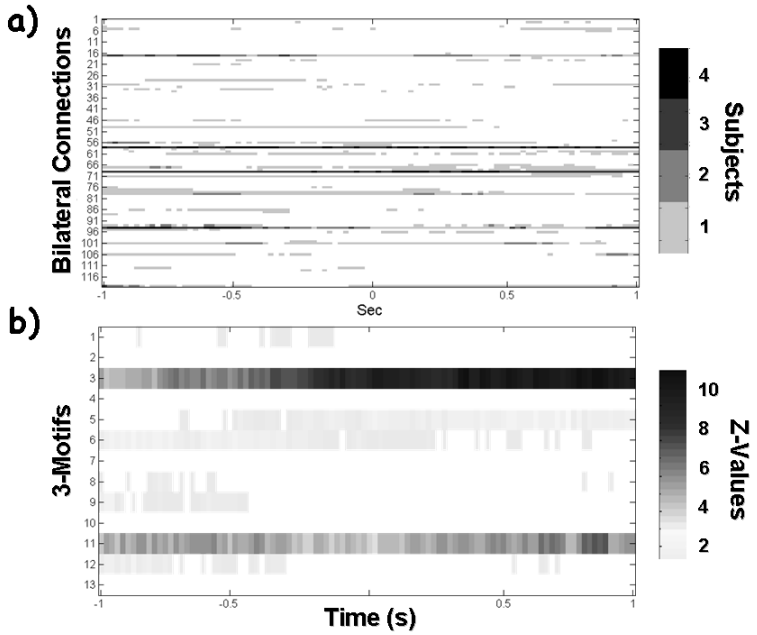

Fig. 10.12. (a) Time-varying persistence of the bilateral connections in the cortical network. On y-axes all the 120 possible reciprocal connections while time in seconds on x-axes. The colour of the line corresponding to a particular link codes the number of subjects that actually hold such a connection. (b) Average time-varying 3-motif spectra. On y-axes all the 13 possible directed 3-motifs are listed while time in seconds is displayed on x-axes.

In Figure 10.12(b), we compared the 3-motif properties of real brain networks with random networks and we identified some motif classes that occurred more frequently during particular stages of the movement. Of particular interest is the involvement of the feed-forward-loop motif (the fifth in the Figure 10.4) that tends to significantly ($p < 0.01$) increase during the proper movement execution (from about 0 to +1 *s*). This type of building block is known to play an important functional role in information processing. In fact, one possible function of this circuit is to activate output only if the input signal is persistent and to allow a rapid deactivation when the input goes off. In the cortical context, a possible interpretation of such a motif would make a particular ROI act as a "switch" for the communication between the others two ROIs composing the triad. Another interesting aspect was revealed by the significant ($p<<0.01$) "persistence" of the single-input motif (the third in the Figure 10.4) that represented the highest recurrent pattern of interconnections during the entire evolution of the foot movement. The main function of this motif is known to involve the "activation" of several parallel pathways by a single activator. Thus, since the single-input

only differs from the feed-forward-loop motif for the functional link between the two areas activated, we can claim the privileged scheme of communication within the functional networks estimated consists in a parallel activation from a particular ROI of two other distinct areas, whose communication seems to increase significantly only during the proper movement execution.

10.5. Conclusions

One of the interesting characteristics of the brain networks presented in this Chapter is that such networks have no precise anatomical support, i.e. there is no particular cerebral structure that implements the network itself. Thus, those brain networks represent functional networks, which could change in topology and properties according to the specific subject's behavior. Another attractive characteristic is that these functional networks are estimated from high-resolution EEG signals. This allows the representation of the graph nodes as particular regions of interest on the cortex. This approach gives to the researcher a "window" to access the brain functions in a different perspective than the usual techniques encountered in the neuroscience literature.

In fact, the development of brain imaging devices (such as the functional Magnetic Resonance Imaging (fMRI), but also the high-resolution EEG technology) often give to the scientist a series of colored hot-spots in the brain that sub-serve the functions performed by the subject during a particular task. Actually, if we look at thousands of fMRI studies a possible impression is that a specific cortical area gets "activated" during the performance of whatever cognitive or motor operation. In this scenario of modern "color phrenology", the study of functional cortical connectivity suggests an image of the brain as a system of objects that rapidly changes the way in which they are interconnected, according to the complexity and to the dynamic of the task proposed to the subject. It is opinion of the Authors that the perspective offered by the use of graph theory to the functional cortical connectivity networks estimated from high-resolution EEG recordings could be a promising way to approach the brain functioning from a modern point of view.

References

Achard S., Salvador R., Whitcher B., Suckling J. and Bullmore, Ed. A Resilient, Low-Frequency, Small-World Human Brain Functional Network with Highly Connected Association Cortical Hubs. The Journal of Neuroscience, 26(1):63–72, 2006.

Akaike H. (1974) A new look at statistical model identification. IEEE Trans Automat Control AC-19:716-723.

Astolfi L., Cincotti F., Mattia D., De Vico Fallani F., Tocci A., Colosimo A., Salinari S., Marciani M.G., Hesse W., Witte H., Ursino M., Zavaglia M., Babiloni F.Tracking the time-varying cortical connectivity patterns by adaptivemultivariate estimators. IEEE Trans Biomed Eng. 55(3):902-13, 2008.

Astolfi L., Cincotti F., Mattia D., Marciani M.G., Baccalà L., De Vico Fallani F., Salinari S., Ursino M., Zavaglia M., Ding L., Edgar J.C., Miller G.A., He B. and Babiloni F. A comparison of different cortical connectivity estimators for high resolution EEG recordings. Human Brain Mapping; 28(2):143-57, 2006.

Babiloni F., Babiloni C., Locche L., Cincotti F., Rossini P.M., Carducci F. High resolution EEG: source estimates of Laplacian-transformed somatosensory-evoked potentials using a realistic subject head model constructed from magnetic resonance images. Med. Biol. Eng. Comput., 38:512-9, 2000.

Babiloni F., Cincotti F., Babiloni C., Carducci F., Basilisco A., Rossini P.M., Mattia D., Astolfi L., Ding L., Ni Y., Cheng K., Christine K., Sweeney J., He B. Estimation of the cortical functional connectivity with the multimodal integration of high resolution EEG and fMRI data by Directed Transfer Function. Neuroimage, 24(1):118-3, 2005.

Baccalà L.A., Sameshima K.., Partial Directed Coherence: a new concept in neural structure determination. *Bio.l Cybern.*, 84: 463-474, 2001.

Barabasi A.L., Albert R. Emergence of scaling in random networks. Science, 286: 509-512, 1999.

Bassett D.S., Meyer-Linderberg A., Achard S., Duke Th., Bullmore E. Adaptive reconfiguration of fractal small-world human brain functional networks. PNAS, 103:19518-19523, 2006.

Bartolomei F., Bosma I., Klein M., Baayen J.C., Reijneveld J.C., Postma T.J., Heimans J.J., van Dijk B.W., de Munck J.C., de Jongh A., Cover K.S., Stam C.J. Disturbed functional connectivity in brain tumour patients: evaluation by graph analysis of synchronization matrices. Clin Neurophysiol; 117:2039-2049, 2006.

Boccaletti S., Latora V., Moreno Y., Chavez M., Hwang D.U. Complex networks: structure and dynamics. Physics Reports, 424:175-308, 2006.

Chávez M., Martinerie J., Le Van Quyen M. Statistical assessment of nonlinear causality: application to epileptic EEG signals. J Neurosci Methods, 124(2):113-28.

De Vico Fallani F., Astolfi L., Cincotti F., Mattia D., Marciani M.G., Salinari S., Kurths J., Gao S., Cichocki A., Colosimo A., Babiloni F. Cortical functional connectivity networks in normal and spinal cord injured patients: Evaluation by graph analysis. Hum Brain Mapp, 28:1334-6, 2007.

De Vico Fallani F., Astolfi L., Cincotti F., Mattia D., Marciani M.G., Tocci A., Salinari S., Witte H., Hesse W., Gao S., Colosimo A., Babiloni F. Cortical network dynamics during foot movements. Neuroinformatics. Spring, 6(1):23-34. 2008.

Eguiluz V.M., Chialvo D.R., Cecchi G.A., Baliki M., Apkarian A.V. Scale-free brain functional networks, Phys. Rev. Lett. 94:018102, 2005.

Garlaschelli D. and Loffredo M.I. Patterns of Link Reciprocity in Directed Networks Phys. Rev. Lett. 93, 268701, 2004.

Hesse W., Möller E., Arnold M., Schack B. The use of time-variant EEG Granger causality for inspecting directed interdependencies of neural assemblies. Journal of Neuroscience Methods 124: 27-44, 2003

Hilgetag C.C., Burns G.A.P.C., O'Neill M.A., Scannell J.W., Young M.P. Anatomical connectivity defines the organization of clusters of cortical areas in the macaque monkey and the cat. Philos. Trans. R. Soc. Lond. B Biol. Sci., 355:91-110, 2000.

Kaminski M., Blinowska K. A new method of the description of the information flow in the brain structures. *Biol. Cybern.* 1991, 65: 203-210.

Kaminski M., Ding M., Truccolo W.A., Bressler S. Evaluating causal relations in neural systems: Granger causality, directed transfer function and statistical assessment of significance. *Biol. Cybern.* 2001, 5, 145-157.

Kus R., Kaminski M., Blinowska K.J. Determination of EEG activity propagation: pair-wise versus multichannel estimate. IEEE Trans. Biomed. Eng. Sep;51(9):1501-10, 2004.

Lago-Fernandez L.F., Huerta R., Corbacho F., Siguenza J.A. Fast response and temporal coherent oscillations in small-world networks, Phys. Rev. Lett.; 84: 2758–61, 2000.

Latora V and Marchiori M. Efficient behaviour of small-world networks. Phys. Rev. Lett. 87:198701, 2001

Latora V. and Marchiori M. Economic small-world behaviour in weighted networks. Eur. Phys. JB 2003; 32:249-263.

Le J. and Gevins A. A method to reduce blur distortion from EEG's using a realistic head model. IEEE Trans Biomed Eng., 40:517-28, 1993.

Micheloyannis S., Pachou E., Stam C.J., Vourkas M., Erimaki S., Tsirka V. Using graph theoretical analysis of multi channel EEG to evaluate the neural efficiency hypothesis. Neuroscience Letters, 402:273-277, 2006.

Milgram, S. *The Small World Problem, Psychology Today* 60-67, 1967.

Milo R., Shen-Orr S., Itzkovitz S., Kashtan N., Chklovskii D. and Alon U. Network motifs: simple building blocks of complex networks Science, 298 824-7, 2002.

Newman M.E.J. The structure and function of complex networks. SIAM Review; 45:167-256, 2003.

Nunez P.L. Neocortical dynamics and human EEG rhythms. New York: Oxford University Press, 708 p., 1995.

Pfurtsheller G., Lopes da Silva F.H. Event-related EEG/EMG synchronizations and desynchronization: basic principles. Clin Neurophysiol. 110:1842–1857, 1999

Salvador R., Suckling J., Coleman M.R., Pickard J.D., Menon D., Bullmore E. Neurophysiological Architecture of Functional Magnetic Resonance Images of Human Brain. Cereb Cortex; 15(9):1332-42, 2005.

Shen-Orr S., Milo R., Mangan S. and Alon U. Network motifs in the transcriptional regulation network of Escherichia coli Nature Genetics, 31 64-8, 2002.

Sporns O., Honey C.J., Kötter R. Identification and classification of hubs in brain networks. PLoS ONE.;2(10):e1049, 2007.

Sporns O., Honey C.J. Small worlds inside big brains. Proc. Natl. Acad. Sci. USA. 19, 103(51):19219-20. 2006.

Stam C.J., Jones B.F., Manshanden I., van Cappellen van Walsum A.M., Montez T., Verbunt J.P., de Munck J.C., van Dijk B.W., Berendse H.W., Scheltens P. Magnetoencephalographic evaluation of resting-state functional connectivity in Alzheimer's disease. Neuroimage; 32:1335-44, 2006.

Stam CJ, Jones BF, Nolte G, Breakspear M, Scheltens Ph. Small-world networks and functional connectivity in Alzheimer's disease. Cereb Cortex; 17:92-99, 2007.

Strogatz SH. Exploring complex networks. Nature; 410:268-76, 2001.

Tononi G., Sporns O., Edelman G.M. A measure for brain complexity: relating functional segregation and integration in the nervous system. Proc. Natl. Acad. Sci. USA, 91:5033-7, 1994.

Watts D.J. and Strogatz S.H. Collective dynamics of 'small-world' networks. Nature, 393:440-2, 1998.